Brain Advance Access published July 19, 2016

BRAIN
A JOURNAL OF NEUROLOGY

Neuroendothelial NMDA receptors as therapeutic targets in experimental autoimmune encephalomyelitis

Richard Macrez,[1,*] Maria C. Ortega,[2,*] Isabelle Bardou,[1] Anupriya Mehra,[1] Antoine Fournier,[1] Susanne M. A. Van der Pol,[3] Benoit Haelewyn,[4] Eric Maubert,[1] Flavie Lesept,[1,‡] Arnaud Chevilley,[1] Fernando de Castro,[2,5] Helga E. De Vries,[3] Denis Vivien,[1] Diego Clemente[2,6,§] and Fabian Docagne[1,§]

[*,§]These authors contributed equally to this work.

Multiple sclerosis is among the most common causes of neurological disability in young adults. Here we provide the preclinical proof of concept of the benefit of a novel strategy of treatment for multiple sclerosis targeting neuroendothelial *N*-methyl-D-aspartate glutamate receptors. We designed a monoclonal antibody against *N*-methyl-D-aspartate receptors, which targets a regulatory site of the GluN1 subunit of *N*-methyl-D-aspartate receptor sensitive to the protease tissue plasminogen activator. This antibody reverted the effect of tissue plasminogen activator on *N*-methyl-D-aspartate receptor function without affecting basal *N*-methyl-D-aspartate receptor activity ($n = 21$, $P < 0.01$). This antibody bound *N*-methyl-D-aspartate receptors on the luminal surface of neurovascular endothelium in human tissues and in mouse, at the vicinity of tight junctions of the blood–spinal cord barrier. Noteworthy, it reduced human leucocyte transmigration in an *in vitro* model of the blood–brain barrier ($n = 12$, $P < 0.05$). When injected during the effector phase of MOG-induced experimental autoimmune encephalomyelitis ($n = 24$), it blocked the progression of neurological impairments, reducing cumulative clinical score ($P < 0.001$) and mean peak score ($P < 0.001$). This effect was observed in wild-type animals but not in tissue plasminogen activator knock-out animals ($n = 10$). This therapeutic effect was associated to a preservation of the blood–spinal cord barrier ($n = 6$, $P < 0.001$), leading to reduced leucocyte infiltration ($n = 6$, $P < 0.001$). Overall, this study unveils a critical function of endothelial *N*-methyl-D-aspartate receptor in multiple sclerosis, and highlights the therapeutic potential of strategies targeting the protease-regulated site of *N*-methyl-D-aspartate receptor.

1 INSERM, INSERM-U919, Caen Cedex, F-14074 France; Université de Caen Basse–Normandie, Caen Cedex, F-14074 France; GIP Cyceron, Caen, F-14074 France
2 Grupo de Grupo de Neurobiología del Desarrollo-GNDe. Hospital Nacional de Parapléjicos – Toledo, Spain
3 Department of Molecular Cell Biology and Immunology, Neuroscience Campus Amsterdam, The Netherlands
4 Centre Universitaire de Ressources Biologiques, Université de Caen Basse-Normandie, Caen, France
5 Grupo de Neurobiología del Desarrollo-GNDe. Instituto Cajal. CSIC – Madrid, Spain
6 Grupo de Neuroinmuno-reparación. Hospital Nacional de Parapléjicos – Toledo, Spain

[‡]Present address: Department of Neuroscience, Physiology and Pharmacology, University College of London, UK

Correspondence to: Fabian Docagne, PhD
Inserm, Inserm UMR-S U919, Centre Cyceron, Bvd H. Becquerel, BP 5229, 14074
Caen Cedex, France
E-mail: docagne@cyceron.fr

Keywords: neuroinflammation; multiple sclerosis; *N*-methyl-D-aspartate receptors; tissue plasminogen activator; Glunomab

Received February 12, 2016. Revised May 6, 2016. Accepted June 2, 2016.

Abbreviations: EAE = experimental autoimmune encephalomyelitis; NMDAR = *N*-methyl-D-aspartate receptor; tPA = tissue plasminogen activator

Introduction

Multiple sclerosis is a demyelinating disease characterized by an alteration of the blood–brain and the blood–spinal cord barriers, and the infiltration of immune cells into the CNS parenchyma, leading to myelin degradation and axonal damage.

Studies in animal models of multiple sclerosis have suggested that excitotoxicity, a toxic process resulting from the excessive activation of glutamatergic receptors, could play a role in this disease (Pitt *et al.*, 2000; Docagne *et al.*, 2007). Accordingly, antagonists of the glutamatergic *N*-methyl-D-aspartate receptors (NMDAR), such as memantine, attenuate white matter damages in experimental multiple sclerosis (Manning *et al.*, 2008). In addition to neurons, where they drive glutamatergic neurotransmission, NMDAR are expressed in a variety of cell types (Skerry and Genever, 2001; Boldyrev, 2005; Verkhratsky and Kirchhoff, 2007; Boldyrev *et al.*, 2013). In particular, brain endothelial cells express NMDAR, which could be involved in blood–brain barrier maintenance and alteration (András *et al.*, 2007; Reijerkerk *et al.*, 2010).

Several regulatory sites exist on the GluN1 subunit of NMDAR. Among them, a protease-regulated site has been identified (Nicole *et al.*, 2001; Fernández-Monreal *et al.*, 2004; Samson and Medcalf, 2006; Benchenane *et al.*, 2007), which leads to the potentiation of NMDAR signalling by the serine-protease tissue plasminogen activator (tPA). Interestingly, tPA was suggested to participate in the pathological features of animal models of multiple sclerosis. For instance, tPA was reported to promote demyelination by activation of plasminogen into plasmin (Cammer *et al.*, 1978) and indirect matrix metalloproteinase (MMP) activation (Cuzner and Opdenakker, 1999). In parallel, tPA was described to promote inflammatory reactions in the CNS by increasing the permeability of the blood–brain barrier (Lopes Pinheiro *et al.*, 2016) and by facilitating monocyte migration through the rat and human blood–brain barrier *in vitro* (Reijerkerk *et al.*, 2008, 2010). Noteworthy, tPA immunoreactivity in post-mortem tissues of patients with multiple sclerosis is associated with inflammatory cells in the perivascular compartment (Cuzner *et al.*, 1996) and tPA activity in the circulation correlates with disease progression (Akenami *et al.*, 1996).

In an earlier study, we showed that the blockade of the protease-regulated site of NMDAR provides therapeutic benefits in an animal model of stroke, an effect associated with reduced blood–brain barrier alteration (Macrez *et al.*, 2011). Also, previous work showed that NMDAR participate in leucocyte transmigration (Reijerkerk *et al.*, 2010). Therefore, we hypothesize that the protease-driven regulation of NMDAR may also play an important role in the pathology of multiple sclerosis.

In this study, we tested a strategy of immuno-intervention aimed at blocking the tPA-induced potentiation of endothelial NMDAR function. Interestingly, this strategy led to a prevention of disease progression in mouse experimental autoimmune encephalomyelitis (EAE). We then show that this therapeutic effect occurs via a direct action on endothelial cells, preventing the alteration of the blood–spinal cord barrier, resulting in a dramatic reduction of immune cell entry into the nervous system and a subsequent preservation of myelin.

Materials and methods

Animals

Male C57BL6/J mice (Janvier) were housed in our local conventional animal facility (CURB, University of Caen). All procedures were performed according to guidelines of the institutional ethics committee (*Comité Normand d'éthique en matière d'expérimentation animale*, CeNomExA). Projects were submitted to this committee for approval in accordance with the European directive no 2010/63/UE (agreement number D14 118 001).

Experimental autoimmune encephalomyelitis

Monophasic EAE was induced in 12-week-old male C57BL6/J mice (Janvier) via subcutaneous immunization with 200 µg recombinant myelin oligodendrocyte glycoprotein ($rMOG_{35-55}$) in an emulsion mixed (volume ratio 1:1) with Complete Freund's Adjuvant (CFA; Difco Laboratories) containing 600 µg of heat-killed *Mycobacterium tuberculosis* H37Ra (Difco). Control animals were injected with saline mixed with CFA containing 600 µg of heat-killed *M. tuberculosis*. All animals were intraperitoneally (i.p.) injected with 200 ng pertussis toxin derived from *Bordetella pertussis* (Sigma-Aldrich) in 200 µl saline at the time of, and 24 h after immunization.

Clinical score

Mice were examined daily for clinical signs of EAE and were scored as follows: 0, no disease; 1, limp tail; 2, hindlimb weakness; 3, complete hindlimb paralysis; 4, hindlimb paralysis plus forelimb paralysis; and 5, moribund or dead. Animals were euthanized if showing a loss of weight of ~10%. Clinical score was assessed daily by one person blinded to the treatment.

Transfection, immunocytochemistry and calcium video imaging in HEK-293 cells

Human embryonic kidney 293 cells (HEK-293 cells) were grown in the presence of reversible NMDA antagonists (200 µM AP5 and 2 mM $MgCl_2$) in a RPMI 1640 medium supplemented with 5% foetal bovine serum. Cells were transfected by the lipofection method (8 µl, FuGENE-6®), with a mixture containing 2 µg of pcDNA3-GluN1–1 b and 2 µg of pcDNA3-GluN2A. For immunostaining experiments, transfected HEK-293 cells were fixed and incubated overnight (4°C) with the Glunomab (1 µg/ml) in PBS with 4% bovine serum albumin (BSA). Finally, cells were incubated with a secondary anti-mouse FITC antibody (1:800) for 1 h at room temperature. Images were taken on a confocal microscope (Leica SP5). For calcium video imaging, cells were loaded in the presence of a HEPES-buffered saline solution containing 10 µM fura-2/AM plus 0.1% pluronic F-127 and 20% solution in dimethyl sulphoxide (30 min, 37°C) and incubated for an additional 45-min period in a HEPES-buffered saline solution. Experiments were performed on the stage of a Leica DMI6000B inverted microscope equipped of a Leica 40× objective. Fura-2 ratio images were digitized using Metafluor® 6.1 software (Universal Imaging Corporation).

Epitope mapping

A total of 141 overlapping pentadecapeptides, frame-shifted by three residues covering the entire amino acid sequence of GluN1 N-terminal domain (residues 19–371). Briefly, peptides were assembled using Fmoc chemistry on a cellulose membrane containing an aminopolyethyleneglycol moiety. The C-terminal residue of each peptide was coupled to the moiety. After Fmoc deprotection, the other amino acids were sequentially added. Finally the side-chain protecting groups were removed by trifluoroacetic acid treatment in the presence of appropriate scavengers, while the linkage of the peptides to the membrane was maintained. Free cysteines were replaced with non-reactive acetamidomethyl cysteines. Purified monoclonal antibodies were incubated on the membrane, and revealed by a classical western blotting method.

Monocyte and T cell migration

Peripheral blood mononuclear cells were isolated from buffy coats obtained from healthy donors (Sanquin Blood Bank, Amsterdam, The Netherlands) using Ficoll density gradient (Lymphoprep™, Axis-Shield). For isolation of monocytes and T cells, we used anti-CD14 magnetic beads (Miltenyi Biotec) with a MACS® MultiStand and LS Column by passing 3 ml of MACS buffer [2 mM EDTA and 0.1% foetal calf serum in phosphate-buffered saline (PBS)] according to the manufacturers' protocol. Human T cell purity was >96% as assessed by expression of CD3 using flow cytometry performed (FACSCalibur™) using CELLQuestTM software (BD Biosciences). Isolated T cells were cultured for 48 h before experiments. Effector T cells were generated by adding IL-2 (10 ng/ml) and phytohaemagglutinin (1 µg/ml) during 48 h (Kooij *et al.*, 2014). The immortalized human brain endothelial cell line hCMEC/D3, which establishes the key features of brain endothelium, was cultured as described previously (Weksler *et al.*, 2005). Migration of primary human monocytes and T cells across confluent monolayers of hCMEC/D3 cells was studied with time-lapse video microscopy as described previously (Mizee *et al.*, 2014). Freshly isolated human monocytes or lymphocytes were added (7.5×10^5 cells/ml) to hCMEC/D3 cells, and the number of migrated cells was assessed after 4 h.

Passive immunization

Injection in the tail vein with the anti-NMDAR monoclonal antibody (15A4B2E5: Glunomab) or control anti-NMDAR monoclonal antibody (6C9B6G11: control isotype) (160 µg in 200 µl each) was performed at the time indicated (Fig. 1A) after EAE onset (MOG). Animals were randomly assigned to the experimental groups. Mortality was null for all procedures/treatments.

Tissue sampling, histology and immunohistochemistry

Three animals from each group were perfused transcardially with 4% paraformaldehyde (PFA) in 0.1 M phosphate buffer, pH 7.4, and their brain and spinal cords were dissected out and post-fixed in the same fixative for 4 h at room temperature. In addition, human post-mortem tissue of non-neurological control cases ($n = 3$) was obtained by rapid autopsy and immediately frozen in liquid nitrogen (The Netherlands Brain Bank, Amsterdam, coordinator Dr Huitinga). The Netherlands Brain Bank received permission to perform autopsies for the use of tissue and for access to medical records for research purposes from the Ethical Committee of the VU University Medical Centre, Amsterdam, The Netherlands. All patients and controls, or their next of kin, had given informed consent for autopsy and use of their brain tissue for research purposes.

In the case of NMDAR immunohistochemistry, the animal underwent perfusion with saline-heparin only (without PFA fixation). After immersion in increasing concentrations of sucrose [until 30% (w/v)], tissue was cut in coronal cryostat sections (20-µm thick: Leica, Nussloch) and thaw-mounted on Superfrost® Plus slide. After several rinses with phosphate buffer, the sections used for all immunohistochemistry experiments except for NMDAR, were pre-treated for 20 min with phosphate buffer containing 3% H_2O_2, 10% methanol (or methanol alone for immunofluorescence experiments) and they were then preincubated for 1 h at room temperature in incubation buffer: 5% appropriate normal serum (Vector) and 0.2% Triton™ X-100 (Merck) diluted in PBS. In the case of NMDAR immunohistochemistry, the tissue sections were post-fixed with 4% PFA for 15 min, blocked with 0.2% BSA in Coon's buffer, and washed in Coon's buffer. Immunohistochemistry was performed by incubating sections overnight at 4°C with the following primary antibodies (diluted in incubation buffer): Glunomab (1:500), polyclonal goat anti-collagen IV antibody (1:1000), monoclonal rat anti-podocalyxin (R&D Systems #192703, 1:250. Kindly provided by Prof. Eduardo Soriano), monoclonal rat anti CD31 (BD #553370, 1:2000), polyclonal goat anti-GluN1 C-terminal antibody GluN1 (Santa Cruz sc1467, 1:100), rabbit

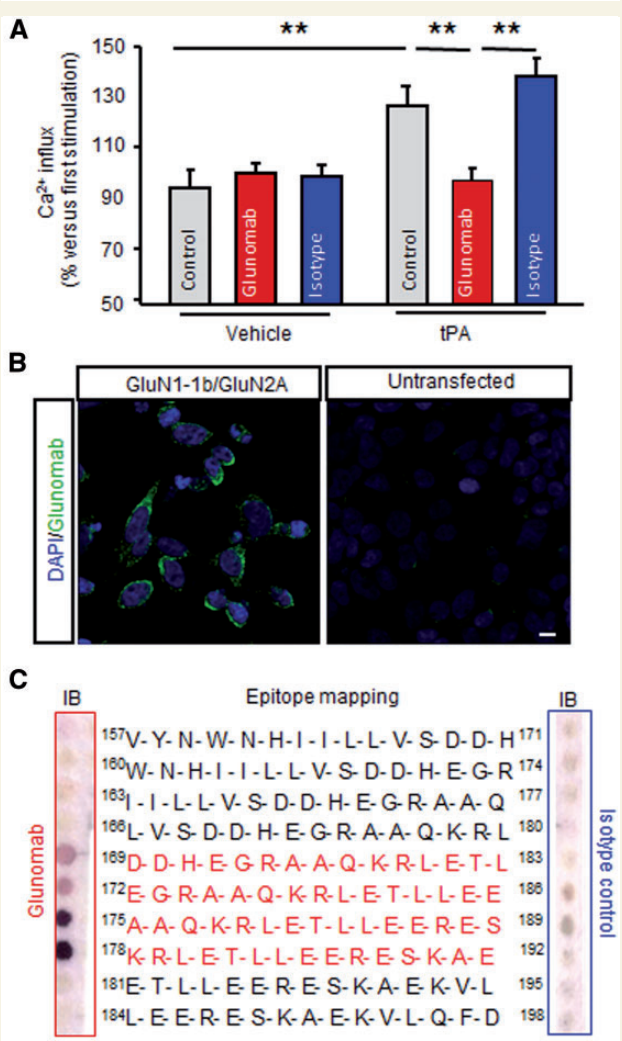

Figure 1 A monoclonal antibody directed against NTD-GluN1 (Glunomab), prevents the potentiation of NMDA-induced calcium influx by tPA. (**A**) Calcium video imaging performed on HEK-293 cells transiently co-transfected with GluN1-1B and GluN2A. After NMDA stimulations (used as baseline), transfected cells were incubated for 20 min with either buffer (control, $n = 20$ cells), tPA (300 nM, $n = 26$), 6C9B6G11 (control isotype) (10 μg/ml, $n = 25$), Glunomab (10 μg/ml, $n = 21$) alone or in combination (tPA + control isotype, $n = 28$; tPA + Glunomab, $n = 30$), prior to a second set of NMDA stimulations. Although antibodies from clone control isotype failed to influence tPA-induced potentiation of NMDA-induced calcium influx, Glunomab completely abolished it (three independent experiments; $^{**}P < 0.01$). (**B**) Illustrative images of immunstaining with Glunomab on HEK-293 cells previously transfected or not with GluN1-1B and GluN2A. Scale bar = 15 μm. (**C**) Immunoblotting of a total of 141 overlapping pentadecapeptides frame-shifted by three residues covering a part of the amino acid sequence of GluN1 NTD (amino acids 19–371) was revealed with Glunomab and control isotype. The figure represents 10 of 141 peptides analysed (amino acids 157–198). Epitope mapping identified the epitope for Glunomab (in red, amino acids 163–192).

monoclonal anti-claudin-5 (Abcam ab131259, 1:1000), rabbit monoclonal anti-occludin (Abcam ab167161, 1:1000) rabbit polyclonal anti-ZO-1 (Abcam ab59720, 1:1000), rat monoclonal anti-CD11b (AbD Serotec MCA74G, 1:250), rat monoclonal anti-Ly-6B.2 (AbD Serotec MCA771G, 1:100), mouse monoclonal anti-MHC-II (eBiosciences 14-5321-81, 1:200,), mouse monoclonal anti-CD11c (eBiosciences 13-0114-81, 1:200), rat monoclonal anti-CD4 (eBiosciences 14-0042 1:25) or tomato lectin (biotinylated, 15 μg/ml, Sigma-Aldrich). The sections were then incubated in buffer containing the corresponding fluorescent secondary antibodies for 1 h at room temperature T (1:1000, Invitrogen). Renaissance® TSA™ Biotin System Kit (PerkinElmer) together with Texas Red®-conjugated Streptavidin (1:200; Jackson Laboratories) was used in the staining procedure for CD11c labelling. The cell nuclei were stained with Hoechst 33342 (10 μg/ml, Sigma-Aldrich). Tomato lectin reaction was detected with Vectastain Elite ABC reagent (Vector Laboratories). The peroxidase reaction product was visualized with 0.05% 3,3′-diaminobenzidine (Sigma-Aldrich) and 0.003% H_2O_2 in 0.1 M Tris-HCl (pH 7.6) and the reaction was monitored under a microscope and terminated by rinsing the slides with phosphate buffer. Eriochrome cyanine for myelin staining was performed as previously described (Moliné-Velázquez *et al.*, 2011).

Confocal imaging and 3D reconstruction

Images of double immunostaining (Collagen IV and Glunomab) were collected using a Leica SP5 confocal microscope with a 100× oil-immersive objective (Leica Microsystems). Confocal images were taken at a 1024 × 1024 pixel resolution with a *z*-step of 0.4 μm.

The 3D structure of the vessel was reconstructed from confocal images using Imaris software (version 5.5, Bitplane, Zurich, Switzerland). Volume and surface functions were used.

Flow cytometry analysis of CNS inflammatory cells

Mice were euthanized and perfused with PBS. Spinal cords were digested with collagenase IV (54 U/ml, Sigma-Aldrich) for 45 min at 37°C, resuspended in 30% Percoll®, and loaded onto 30/70% Percoll® gradient. After centrifuge at 1300*g* for 30 min, myelin was removed from the top of the gradient and the CNS inflammatory cells were collected in PBS. Cells (10^5) were resuspended in 50 μl of staining buffer (sterile PBS supplemented with 1% BSA, 1% foetal bovine serum) and the Fc receptors were blocked for 10 min at 4°C with anti-CD16/CD32 antibodies (BD Biosciences 553142, 10 μg/ml). After blocking, the cells were labelled with various fluorochrome-conjugated monoclonal antibodies: anti-mouse CD11b PerCP Cy5.5 (BD Biosciences 550993), anti-mouse F4/80-eFluor 450 (eBiosciences 48-4801-82) and anti-mouse CD3ε APC (BD Biosciences 553066). CNS inflammatory cells were washed twice with staining buffer, they were recovered by centrifugation at 1500 rpm for 5 min at room temperature, resuspended in PBS and finally, the samples were assayed in a FACSCanto™ II cytometer (BD Biosciences). The data were analysed with FlowJo 7.6.4 software (TreeStar Inc.)

Statistical analyses

Results are presented as mean ± standard error of the mean (SEM). For calcium video imaging of HEK-293 cells, the responsiveness was analysed by Wilcoxon signed-rank test to compare pre-and post-incubation response. In addition, for group comparison, Kruskal-Wallis tests were used followed by Mann-Whitney U-tests as *post hoc* tests. Other statistical analyses were performed by the Kruskall-Wallis' test, followed by *post hoc* comparison with the Mann-Whitney's test.

Results

Design of a blocking monoclonal antibody directed against the protease-regulated site of NMDAR

The main goal of this study was to elaborate a strategy of immune-intervention directed against the site of interaction of tPA with NMDAR. To this end, we developed a monoclonal antibody directed against the precise site of interaction of tPA with NMDAR, which could prevent the effects of tPA on NMDAR function. We first screened a series of monoclonal antibodies generated using the recombinant N-terminal domain (residues 19–371) of GluN1 NTD as antigen. Positive antibodies on ELISA for GluN1-NTD (data not shown) were then selected for their ability to block the potentiating effects of tPA on NMDAR function as assessed by calcium imaging in HEK-293 cells engineered to express NMDAR (Fig. 1). One clone (15A4B2E5: Glunomab) was chosen on this functional basis (Fig. 1A and Supplementary Fig. 1A). In transfected HEK-293 cells, tPA (300 nM) increased NMDA-induced Ca^{2+} influx by ~40%. Noteworthy, the co-application of Glunomab prevented this effect of tPA (Fig. 1A; $P < 0.01$), while Glunomab did not influence NMDA-evoked signalling in the absence of tPA (Fig. 1A). As expected, Glunomab stained HEK-293 cells transfected with GluN1, but not untransfected cells (Fig. 1B). Another clone, 6C9B6G11 (control isotype, Supplementary Fig. 1A and B), failed to block tPA-mediated potentiation of NMDAR function (Fig. 1A) and was used as a control isotype throughout the rest of the study. Epitope mapping showed that Glunomab epitope was localized between amino acids 169 and 192 of GluN1 sequence (Fig. 1C). This portion of GluN1 sequence is fully conserved between mouse, rat and human (data not shown).

Glunomab prevents leucocyte transmigration through the blood–brain barrier *in vitro*

We used a human *in vitro* model of the blood–brain barrier (hCMEC/D3 cells; Weksler *et al.*, 2005) to test the ability of Glunomab to block leucocyte transmigration. First, we confirmed that Glunomab antibody was able to stain NMDAR on endothelial cells in this model (Fig. 2A). We next showed that, under inflammatory condition (TNF treatment), Glunomab significantly blocked human monocyte migration (+50% of migrated monocytes for TNF alone compared to basal condition and −63% of migrated monocytes for the condition TNF + Glunomab compared to TNF alone; $n = 12$, $P < 0.05$; Fig. 2B). tPA treatment increased the transendothelial migration of human monocytes in non–inflammatory condition and in the presence of TNF (+38% compared to control and 16% compared to TNF condition, respectively; $n = 12$, $P < 0.05$; Fig. 2C). Importantly, Glunomab antibody was also able to block the increase in human monocyte migration induced by tPA treatment (+38% of migrated monocytes for TNF + tPA compared to TNF alone, −53% of migrated monocytes for TNF + tPA + Glunomab compared to TNF + tPA and −38% of migrated monocytes for TNF + tPA + Glunomab compared to TNF + tPA + control isoptype; $n = 12$, $P < 0.05$ Fig. 2D). This effect was not limited to monocyte migration, as it also significantly blocked human T cell migration using similar conditions (+70% of migrated T cells for TNF as compared to basal condition and −58% of migrated T cells for TNF + tPA + Glunomab as compared to TNF + tPA; $n = 12$, $P < 0.05$; Fig. 2E). Control isotype displayed limited, non-significant effects in these experiments (Fig. 2B, D and E).

Glunomab binds to NMDAR in the vicinity of neuroendothelial tight junctions of the blood–spinal and blood–brain barrier

Based on these *in vitro* data, our next step was to test if Glunomab was able to bind and stain NMDAR on spinal cord endothelium. We observed a positive immunostaining with Glunomab on mouse spinal cord microvessels of control animals (Fig. 3A). A similar pattern of staining was observed when using an antibody directed against the C-terminal end of GluN1 (Fig. 3A). Glunomab also revealed endothelial NMDAR in human tissues (Fig. 3B). Interestingly, Glunomab revealed NMDAR co-localized with the tight junction proteins claudin 5, occludin 1 and zona occludens 1 on mouse spinal cord endothelium (Fig. 3C and Supplementary Fig. 2A). Similar pattern of expression and co-localization was observed on mouse brain microvessels (Supplementary Fig. 2B). In contrast, no staining was observed with Glunomab in brain microvessels devoid of tight junctions, such as fenestrated capillaries of the external zone of the median eminence (Fig. 3D and Supplementary Fig. 3). These data show that NMDAR are expressed on tight junction-containing, blood–brain/blood–spinal cord barrier-forming endothelial cells. Using confocal microscopy after co-immunostaining of Glunomab with collagen IV and podocalyxin, a marker of luminal

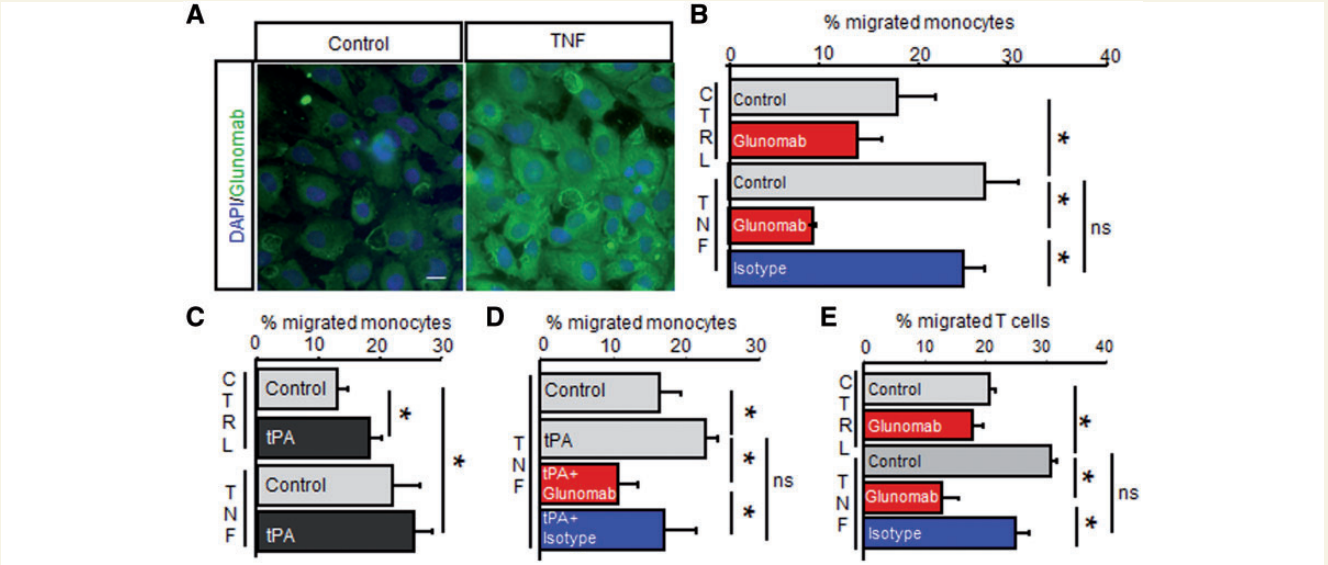

Figure 2 Glunomab prevents immune cell transmigration through the blood–brain barrier *in vitro*. (**A**) Illustrative picture of Glunomab staining on endothelial cells (hCMEC/D3 cells) on basal condition (control) and after TNF stimulation (*right*). Scale bar = 15 μm. (**B**) Human monocyte migration across hCMEC/D3 endothelial cells; effect of Glunomab on control and TNF treated endothelial cells compared to control isotype ($n = 12$ in each condition, three independent experiments; $^*P < 0.05$). (**C**) Human monocyte migration across TNF treated hCMEC/D3 endothelial cells and the added effect of tPA ($n = 12$ in each condition, three independent experiments; $^*P < 0.05$). (**D**) Human monocyte migration across TNF treated human brain endothelial cells and the added effect of tPA plus inhibition by Glunomab compared to control isotype ($n = 12$ in each condition, three independent experiments; $^*P < 0.05$). (**E**) Human T cell migration across hCMEC/D3 endothelial cells; effect of Glunomab on control and TNF treated endothelial cells compared to isotype ($n = 12$ in each condition, three independent experiments; $^*P < 0.05$). ns = non-significant.

surface, and 3D image reconstruction, we were able to show that endothelial NMDAR are located at the luminal surface of CNS endothelium (Fig. 4 and Supplementary Video 1).

Glunomab stops symptom progression in EAE by preventing blood–spinal cord barrier leakage and immune cell infiltration

The above data show that Glunomab is able to block immune cell migration across neurendothelial cells *in vitro* and that this antibody binds NMDAR expressed on the neuroendothelium *in vivo*. We thus hypothesized that Glunomab could provide therapeutic effects in experimental multiple sclerosis. Based on this, we then tested the effects of Glunomab in MOG-induced EAE. Our first approach was to perform three intravenous injections of Glunomab (160 μg per mouse) at the onset, the effector phase and the chronic phase of EAE. This treatment led to a general reduction of clinical score throughout the disease ($P < 0.001$ from Day 6 post-onset to the end of treatment, Fig. 5A), illustrated by a reduced cumulative clinical score (36.7 ± 5.5 versus 72.4 ± 14; $n = 24$ mice per group, $P < 0.001$; Fig. 5B) and a reduced mean peak score (1.9 ± 0.37 for Glunomab treated mice versus 3.4 ± 0.44 for the isotype control; $n = 24$ mice per group, $P < 0.001$; Fig. 5C). We then tested the therapeutic efficacy of a single injection of Glunomab performed during the effector phase of the disease. This single injection was enough to provide a conspicuous therapeutic effect characterized by a complete blockade of disease progression (Fig. 5D, $P < 0.001$ from Day 9 post-onset to the end of treatment), illustrated by a reduced cumulative clinical score (63.4 ± 2.2 versus 41.3 ± 3.3, $n = 24$ per group, $P < 0.001$; Fig. 5E) and a reduced mean peak score (2.2 ± 0.56 for Glunomab treated mice versus 3.9 ± 0.18 for the isotype control; $n = 24$ mice per group, $P < 0.001$; Fig. 5F). Noteworthy, in tPA knockout animals, Glunomab did not induce any modification of clinical score throughout the disease (Supplementary Fig. 4A), cumulative clinical score (Supplementary Fig. 4B) or mean peak score (Supplementary Fig. 4C).

Histological analysis showed that mice treated with Glunomab displayed a dramatically reduced demyelination within inflammatory lesions ($14.69\% \pm 2.05\%$ for EAE mice treated with the control isotype antibody versus $0.3\% \pm 0.1\%$ for EAE mice treated with Glunomab; $n = 6$, $P < 0.001$; Fig. 5G–I).

One week after the injection of the isotype antibody during the effector phase of EAE, we observed a classical pattern of endothelium activation characterized by the expression of tomato lectin and VCAM-1 on microvessels of the spinal cord (Fig. 6A and B), together with an increase in

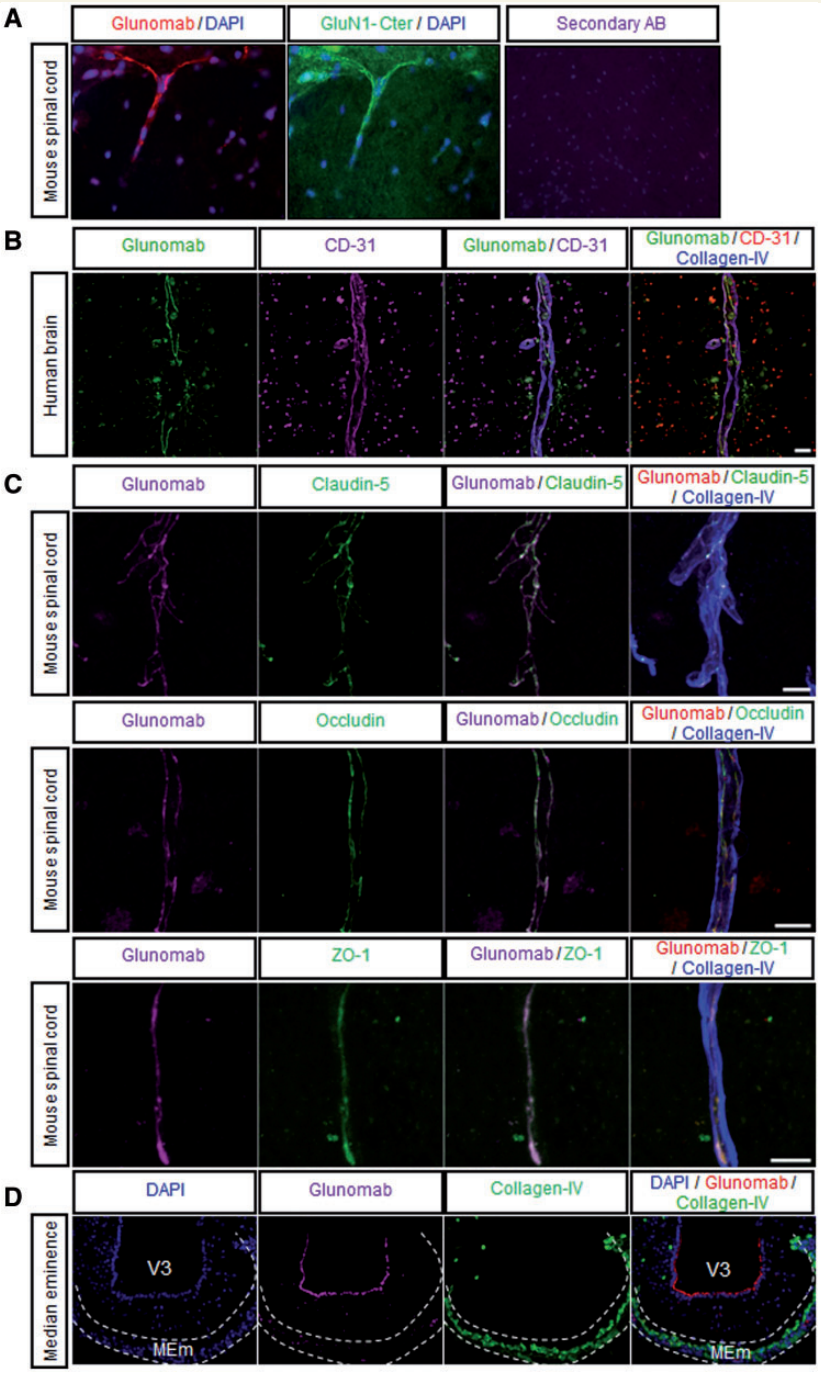

Figure 3 NMDAR co-localized with tight junction proteins on endothelial cells at the blood–spinal cord barrier. (**A**) Photomicrographs show immunostaining from parallel sections for GluN1 subunit on endothelial cells in a blood vessel on the spinal cord of sham mice by immunofluorescent staining with Glunomab (directed to N-terminal domain of GluN1, in red) and anti-C-terminal domain of GluN1 (GluN1-Cter, in green). Scale bar = 10 μm. (**B**) Confocal photomicrographs show immunostaining for Glunomab (green), CD 31 (red) and collagen IV (blue) in human brain. Scale bar = 20 μm. (**C**) Confocal photomicrographs show immunostaining for Glunomab (red), collagen IV (blue) and claudin-5 (green, scale bar = 10 μm), occludin (green, scale bar = 10 μm) and ZO-1 (green, scale bar = 5 μm) in the spinal cord of sham mice. (**D**) Photomicrographs show immunostaining for Glunomab (in red), and collagen-IV (green) in naïve mice. Note the absence of Glunomab staining in vessels of the external zone of the median eminence (MEm). V3 = third ventricle. Scale bar = 50 μm.

the permeability of the blood–spinal cord barrier reflected by fibrinogen leakage into the perivascular parenchyma (Fig. 6A and B). In contrast, treatment with Glunomab resulted in a drastic reduction of immunostaining for tomato lectin and VCAM1 on microvessels and for fibrinogen in the spinal cord parenchyma (−42%, −94% and −84%, respectively compared to control isotype treatment, $P < 0.01$; Fig. 6A and B). These data suggest that

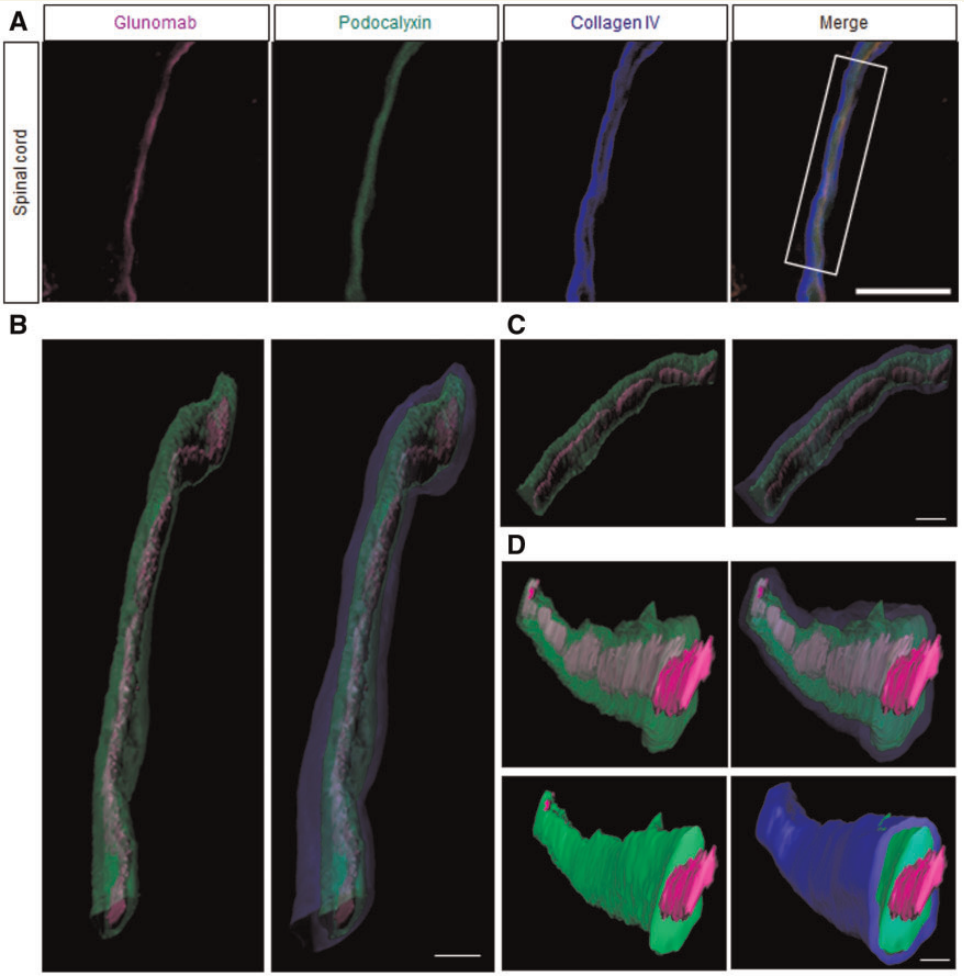

Figure 4 NMDAR displayed at the luminal surface of neurovascular endothelium. Confocal analysis of Glunomab staining (magenta) location in a collagen IV (blue) and podocalyxin (green) labelled white matter capillary. (**A**) Image of a longitudinal capillary showing Glunomab immunostaining in a luminal location with respect to the collagen and podocalyxin immunoreactivity of the endothelial cells. (**B**) Tridimensional reconstruction from the capillary showed in **A** (section indicated with white box), top view. (**C**) Tridimensional reconstruction from the capillary showed in **A** (section indicated with white box), side view. (**D**) Perpendicular view of the solid 3D reconstruction of the capillary showed in **A**. Scale bars: **A** = 10 μm; **B** and **D** = 2 μm; **C** = 3 μm.

Glunomab acts on the neurovasculature in EAE by restoring blood–spinal cord barrier function.

We next asked whether this action on blood–spinal cord barrier functions could lead to modifications of immune cell entry towards the parenchyma in EAE mice. Flow cytometry analysis showed a reduction in both myeloid and lymphoid populations in the spinal cord of MOG-induced EAE mice when treated with a single injection of the Glunomab (Fig. 7A and B). These data were confirmed by histological analysis of the demyelinated area of the spinal cord, with drastic reductions in the number of $CD11b^+$ (macrophages/microglia), $Ly6B.2^+$ (neutrophils), MHC-II^+ (antigen-presenting cells), $CD11c^+$ (dendritic cells) and $CD4^+$ (T4 lymphocytes) cells (Fig. 7C and D) in EAE mice treated with the Glunomab [−86%, −100% (non-detected), −79%, −90% and −100% (v), respectively compared to control isotype treatment; $n = 6$ mice per group, $P < 0.001$; Fig. 7D]. Flow cytometry analysis from spleens showed that Glunomab treatment did not influence lymphocyte activation (Supplementary Tables 1 and 2).

Discussion

The present study reports the therapeutic effects of a strategy of immunointervention targeting neuroendothelial NMDAR in experimental multiple sclerosis. Blocking the action of the serine protease tPA on NMDAR by using a novel monoclonal antibody (Glunomab) results in a reduced severity of the disease with a drastic reduction of inflammation and demyelination. Glunomab targets endothelial cells and leads to a reduced transmigration of immune cell through the blood–spinal cord barrier, which sustains its therapeutic effects. Glunomab is effective when

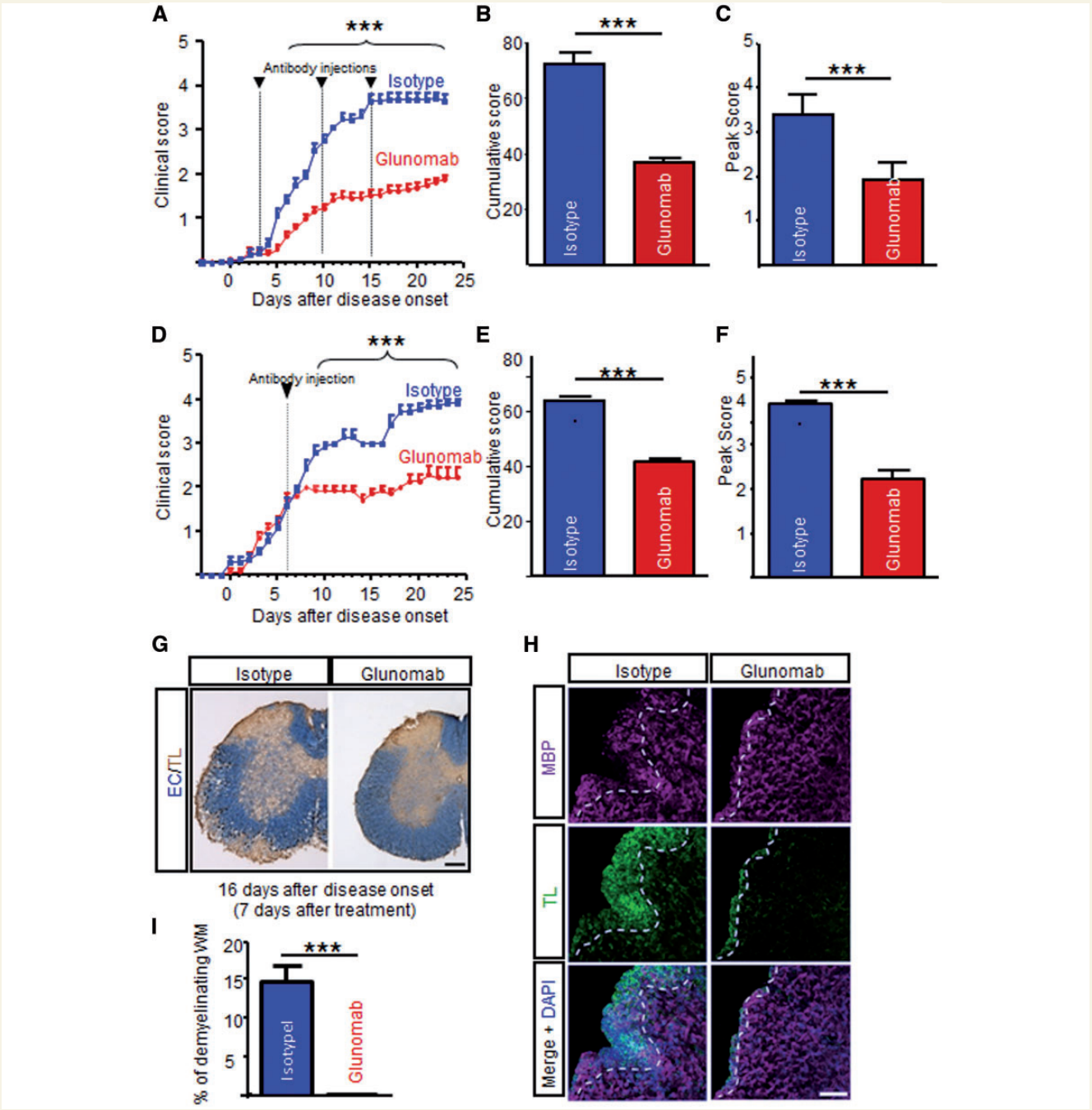

Figure 5 Glunomab stops the progression of MOG-EAE. (**A**) MOG-EAE mice were injected with Glunomab (red line, 160 μg) or control isotype (blue line, 160 μg) 3, 10 and 15 days after the onset of symptoms. Clinical score was assessed daily by one examiner blinded to the treatment ($n = 24$ per group; $^{***}P < 0.001$). (**B**) Histrogram shows cumulative clinical score (mean ± SEM) for glunomab and control isotype groups. $^{***}P < 0.001$. (**C**) Histogram shows mean score at the peak of disease (mean ± SEM) for Glunomab and control isotype groups. $^{***}P < 0.001$. (**D**) MOG-EAE mice were injected with Glunomab (red line, 160 μg) or control isotype (blue line, 160 μg) 6 days after the onset of symptoms. Clinical score was assessed daily by one examiner blinded to the treatment ($n = 24$ per group, $^{***}P < 0.001$). (**E**) Histogram shows cumulative clinical score (mean ± SEM) for Glunomab and control isotype groups. $^{***}P < 0.001$. (**F**) Histogram shows mean score at the peak of disease (mean ± SEM) for Glunomab and control isotype groups. $^{***}P < 0.001$. (**G**) *Left*: Illustrative example of spinal cord of isotype injected mice (7 days after injection) clear demyelinating areas [eriochrome cyanine (EC) staining, bordered with a dashed line] filled with tomato lectin (TL)-positive cells. *Right*: Representative image of spinal cord of Glunomab injected mice (7 days after injection) showing no signs of overt demyelination or tomato lectin staining. Scale bar = 500 μm. (**H**) Immuno-fluorescent staining for myelin basic protein (MBP, magenta) and tomato lectin (TL, green) in spinal cord tissue derived from EAE-mice treated with isotype antibody or treated with Glunomab 16 days after disease onset (7 days after glunomab or isotype treatment). Scale bar = 60 μm. (**I**) Histogram representing the percentage of demyelinated area/white matter area for Glunomab-treated mice compared to isotype treated mice ($n = 6$ mice per group, $^{***}P < 0.001$; ND = non-detected).

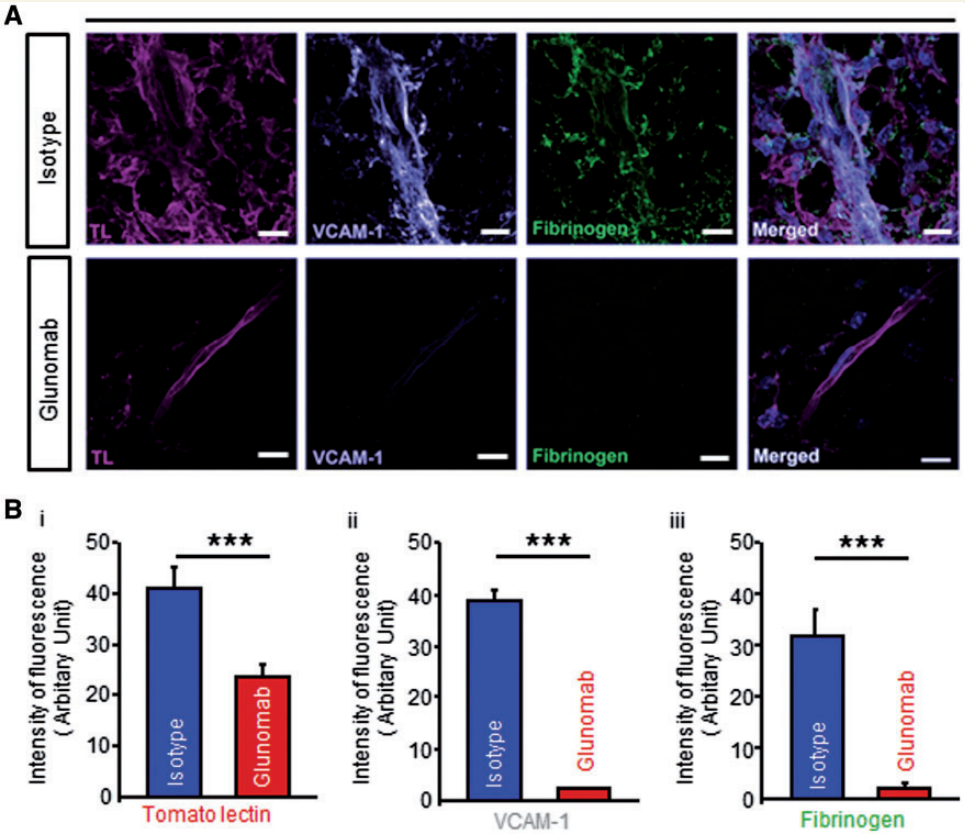

Figure 6 Glunomab drastically reduces endothelial activation and BSCB leakage. (**A**) Immuno-fluorescent staining of Tomato- Lectin (TL; magenta), VCAM-1 (white) and fibrinogen (green) in spinal cord tissue derived from EAE-mice treated with isotype antibody or treated with Glunomab 16 days after disease onset (7 days after glunomab or isotype treatment). Scale bar = 50 μm. (**B**) Histograms show quantification of intensity of fluorescence of (**i**) TL, (**ii**) VCAM1 and (**iii**) fibrinogen in the spinal cord of EAE mice (16 days after disease onset and 4 days after Glunomab (red bars) or control isotype (blue bar) treatment (arbitrary units, $n = 6$ mice per group, $^{***}P < 0.001$).

injected during the effector phase of EAE, in symptomatic animals (clinical score 2). Noteworthy, this timing of treatment corresponds to a stage of ongoing blood–brain barrier and blood–spinal cord barrier alterations (Floris *et al.*, 2004), which is compatible with the proposed mechanism of action on blood–brain/blood–spinal cord barriers. In addition to this, Glunomab binds the luminal surface of the neurovascular endothelium, in the vicinity of tight junction proteins. This sustains the proposed mode of action, which resides in a blockade of blood–brain/blood–spinal cord barrier alterations and subsequent entry of immune cells into the parenchyma.

We describe that NMDARs are localized at the luminal surface of neurovascular endothelium, in relation to tight junction proteins zona occludens 1, claudin 5 and occludin. This complements the previous observation of NMDAR in cultured human brain endothelial cells, as well as *in vivo*, in the mouse brain vasculature (Reijerkerk *et al.*, 2010).

The fact that NMDAR are displayed by endothelial cells raises the question of their function. Our study highlights their role in the regulation of the blood–spinal cord barrier during neuroinflammatory conditions. Previous reports showed that EAE symptoms were reduced by the voltage-dependent NMDAR antagonist memantine (Paul and Bolton, 2002; Sulkowski *et al.*, 2013), together with a reduced blood–brain barrier permeability. However, the ultimate mechanisms involved are not fully understood. NMDAR activation could lead to blood–brain or blood–spinal cord barrier permeability by alteration of occludin expression and distribution (András *et al.*, 2007) or mitochondrial toxicity (Kamat *et al.*, 2015). Production of reactive oxygen species (Sharp *et al.*, 2003; Scott *et al.*, 2007) and polyamines (Bolton and Paul, 2006), rise in intracellular calcium (Sharp *et al.*, 2003) or activation of intracellular kinases (Basuroy *et al.*, 2006) have all been proposed as potential mediators of this effect. All of these processes are known mediators of excitotoxicity in neurons, which suggests that endothelial NMDAR-induced blood–brain or blood–spinal cord barrier permeability could share features with neuronal NMDAR-induced excitotoxic death. Beyond these toxic effects due to excessive stimulation of NMDAR, a physiological pathway mediated by NMDAR must exist in endothelial cells. The role of this physiological pathway and its precise description should be addressed in further studies.

The observation that Glunomab staining is strongly increased upon TNF treatment *in vitro* in hCMEC/D3

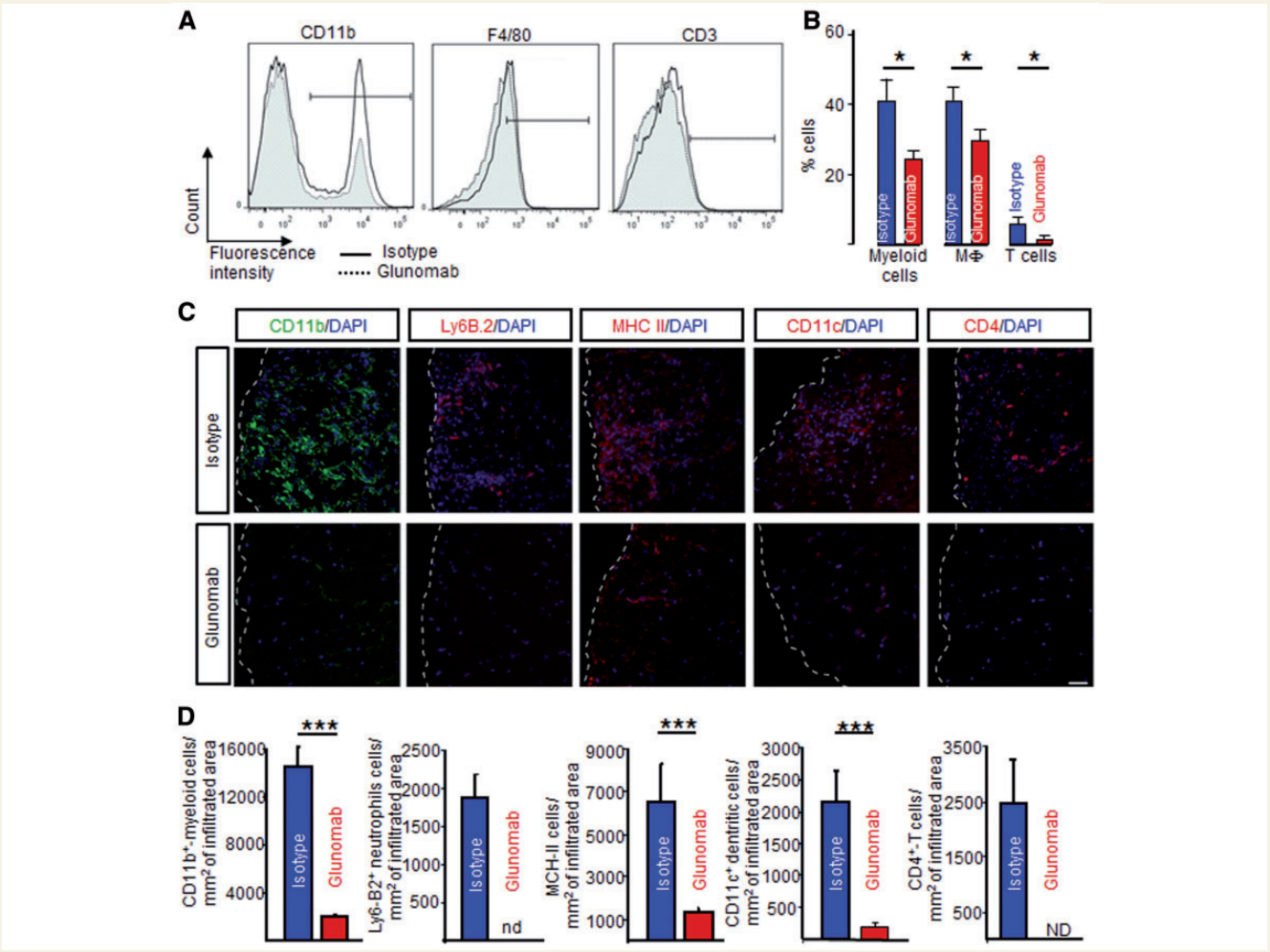

Figure 7 The treatment with Glunomab abolishes immune cell infiltration in the spinal cord of EAE mice. (**A** and **B**) Flow cytometry analysis of immune cell populations within the whole spinal cord from control isotype or Glunomab injected EAE mice 16 days after disease onset (7 days after Glunomab or isotype treatment). Glunomab treatment induced a decrease in the percentage of the whole myeloid ($CD11b^+$), macrophage (MF, $CD11b^+F4/80^+$ cells) and lymphoid ($CD3^+$ T cells) subsets extracted from the spinal cord. (**C**) Photomicrographs show immunostaining in thoracic spinal cords immunolabelled for CD11b (myeloid cells), Ly-6B.2 (neutrophils), MHC-II (antigen presenting cells), CD11c (dendritic cells) and CD4 (T4 lymphocytes). (**D**) Histograms show quantification of cell infiltration in the spinal cord of EAE mice after Glunomab (red bars) or control isotype (blue bars) treatment (expressed in number of cells/mm^2 of infiltrated areas, $n = 6$ mice per group, $^{***}P < 0.001$, ND = non-detected).

cells suggests that NMDAR expression by brain endothelium is upregulated in inflammatory conditions. If this is confirmed by further *in vivo* studies, this would suggest that NMDAR expression on endothelial cells could be part of the endothelium activation that occurs during inflammation, together with the expression of cell adhesion molecules. On a functional point of view, this would mean that NMDAR effects on leucocyte transmigration would be silenced in non-inflammatory conditions and unveiled during inflammation. In addition, endothelial NMDAR expression could also be a marker of endothelial activation during inflammation and could be targeted by diagnostic tools such as molecular MRI for instance.

Another important issue is the origin of the endogenous ligands which activate endothelial NMDAR. Platelets (Tremolizzo *et al.*, 2006), monocytes (Lee *et al.*, 2011) and lymphocytes (Garg *et al.*, 2008) release glutamate. Of note, glutamate plasma levels are elevated in patients with multiple sclerosis, as compared to control patients (Pampliega *et al.*, 2008). These data suggest that leucocyte-derived glutamate could be responsible for NMDAR activation in multiple sclerosis.

Our data suggest that endogenous tPA is involved in the neuroinflammatory processes during EAE. This comes in complement to recent observations of a deleterious, pro-inflammatory effect of exogenously administered tPA in the same model (Wang *et al.*, 2014). Previous studies using tPA knockout mice had described a dual role for endogenous tPA in EAE: tPA was suggested to participate in leucocyte infiltration during the onset and effector phase

of EAE (delayed lymphocyte infiltration in tPA knock-out animals) (Cuzner *et al.*, 1996), and to protect axons via parenchymal fibrinolysis during the recovery phase of EAE (fibrin accumulation on damaged axons in tPA knock-out animals) (Akenami *et al.*, 1996). These studies in knock-out animals did not allow discrimination between the multiple effects of tPA, in particular between NMDAR-dependent and NMDAR-independent effects, which can explain the dual effects observed. The strategy used in the present study allows selective blockade of NMDAR- dependent effects of tPA at specific time points of EAE. By using this strategy, we show here that tPA, by acting on NMDAR during the effector phase of EAE, promotes leucocyte infiltration through the blood–spinal cord barrier.

tPA effects on blood–brain barrier function, though never addressed before in multiple sclerosis models, have been previously studied in the context of stroke. In endothelial cells, tPA induces LRP signalling through NF-κB to induce the synthesis of metalloproteinases MMP9 and MMP3, which in turn contribute to blood–brain barrier breakdown and intracranial bleeding (Wang *et al.*, 2003; Suzuki *et al.*, 2009). In parallel, tPA, through LRP shedding (Polavarapu *et al.*, 2007) on perivascular astrocytes, induces the expression of MMP9 (Wang *et al.*, 2006), and promotes the detachment of astrocyte end-feet processes (Polavarapu *et al.*, 2007). Our present results suggest that the mechanisms of action of tPA in EAE differ from what previously described in experimental stroke: in EAE, particularly during the effector phase, tPA would act on endothelial NMDAR to sustain leucocyte infiltration, as it was previously suggested in a cell culture model of blood–brain barrier (Reijerkerk *et al.*, 2010). This difference in the mechanism is consistent with the idea that blood–brain barrier breakdown in stroke and its animal models is different from blood–brain barrier/blood–spinal cord barrier alteration in multiple sclerosis and its animal models, in terms of cause, characteristics, timing, intensity and consequences (Obermeier *et al.*, 2013). Our study shows the relevance of this newly-described mechanism in an appropriate animal model.

Two recent studies allow hypothesizing on the pathway which links tPA, NMDAR and leucocyte transmigration: Wang *et al.* (2014) reported that tPA upregulates ICAM-1 expression in brain endothelial cells through an action dependent on the LRP1 receptor (a tPA receptor); and Mantuano *et al.* (2013) showed that LRP1 associates with NMDAR to trigger cell signalling in Schwann cells. This suggests that in endothelial cells, tPA, through a signalling pathway dependent on the association of LRP1 and NMDAR, could increase the expression of cell adhesion molecules, which would facilitate leucocyte transmigration.

The main described source of tPA is endothelial cells, which suggests that tPA could act in an autocrine fashion on endothelial NMDAR. Another exciting hypothesis is that immune cells could produce tPA during the processes of adhesion/transmigration, which would act as a signal for endothelial cells via endothelial NMDAR. In fact, neutrophils and macrophages have been shown to produce tPA, which in turn can promote their recruitment to the sites of inflammation (Lin *et al.*, 2014; Uhl *et al.*, 2014). In accordance with this, neutrophils have been shown to mediate blood–spinal cord barrier opening in EAE (Aubé *et al.*, 2014). The drastic reduction of immune cell infiltration to the spinal cord of the animals treated with Glunomab, observed in the present study, is in favour of this hypothesis.

Anti-NMDAR antibodies are present in subpopulations of patients with CNS diseases, the prototype of which being anti-NMDAR encephalitis (Dalmau *et al.*, 2008), and are known to be pathogenic in most cases. Nevertheless, Glunomab targets a different region of NMDAR than the epitope targeted in anti-NMDAR encephalitis (N368/G369) (Gleichman *et al.*, 2012). On a functional point of view, antibodies from anti-NMDAR encephalitis patients reduce basal NMDAR function (Mikasova *et al.*, 2012), while Glunomab does not, but rather reduces the potentiation of this response by tPA (Fig. 1A). This absence of effect on basal NMDAR function is likely to impede toxic effects of our antibody on physiological glutamatergic transmission.

The development of this site-specific antibody against the tPA/NMDAR binding site provides hopes for efficient translation to the clinical situation. NMDAR function is crucial for various physiological processes, such as normal synaptic transmission. For that reason, unacceptable side effects have been reported from clinical trials using compounds that fully block NMDAR. Thus, compounds targeting modulatory sites on the NMDAR without affecting basal NMDAR transmission are expected to promote therapeutic effects without the unacceptable side effects. The monoclonal antibody developed in this study fulfils this criterion, as it can block the potentiating effects of tPA on NMDAR, rather than fully inhibit NMDAR-mediated processes. This makes of our novel antibody-based strategy a promising new therapeutic tool for diseases in which tPA/NMDA interactions are causal of tissue damage, including multiple sclerosis.

Acknowledgements

We express our gratitude to Claudine Fauchon and Iris Sánchez for their excellent technical assistance. We deeply thank Dr José Ángel Rodríguez-Alfaro and Dr Javier Mazario for their help with the confocal imaging, and Dr Virgina Vila-del Sol for her help with flow cytometry analysis. We are grateful to Pr Eduardo Soriano for his useful advices concerning Podocalyxin immunostaining.

Funding

This work was funded by the European Union via the FP7 programme, by the *Association pour la Recherche sur la Sclérose en Plaques* (ARSEP Special Call

"*Immunointervention in demyelinating diseases of the Central Nervous System*") and by the *Fondation pour la Recherche Médicale* (FRM). A.M. is an ITN-Marie Curie fellow (European Union). R.M. received a postdoc fellowship from the *Association pour la Recherche sur la Sclérose en Plaques* (ARSEP). F.L., A.C. and A.F. were financed by the help of the Regional Council of Lower-Normandy (CRBN). M.C.O. was hired under an ARSEP grant. F.d.C. is a CSIC Staff Scientist and received special permission to be hired by the Gobierno de Castilla-La Mancha/SESCAM (Spain). D.C. is hired by the Gobierno de Castilla-La Mancha/SESCAM.

Supplementary material

Supplementary material is available at *Brain* online.

References

Akenami FO, Sirén V, Koskiniemi M, Siimes MA, Teräväinen H, Vaheri A. Cerebrospinal fluid activity of tissue plasminogen activator in patients with neurological diseases. J Clin Pathol 1996; 49: 577–80.

András IE, Deli MA, Veszelka S, Hayashi K, Hennig B, Toborek M. The NMDA and AMPA/KA receptors are involved in glutamate-induced alterations of occludin expression and phosphorylation in brain endothelial cells. J Cereb Blood Flow Metab 2007; 27: 1431–43.

Aubé B, Lévesque SA, Paré A, Chamma É, Kébir H, Gorina R, et al. Neutrophils mediate blood-spinal cord barrier disruption in demyelinating neuroinflammatory diseases. J Immunol 2014; 193: 2438–54.

Basuroy S, Seth A, Elias B, Naren AP, Rao R. MAPK interacts with occludin and mediates EGF-induced prevention of tight junction disruption by hydrogen peroxide. Biochem J 2006; 393: 69–77.

Benchenane K, Castel H, Boulouard M, Bluthé R, Fernandez-Monreal M, Roussel BD, et al. Anti-NR1 N-terminal-domain vaccination unmasks the crucial action of tPA on NMDA-receptor-mediated toxicity and spatial memory. J Cell Sci 2007; 120: 578–85.

Boldyrev AA. Homocysteinic acid causes oxidative stress in lymphocytes by potentiating toxic effect of NMDA. Bull Exp Biol Med 2005; 140: 33–7.

Boldyrev A, Bryushkova E, Mashkina A, Vladychenskaya E. Why is homocysteine toxic for the nervous and immune systems? Curr Aging Sci 2013; 6: 29–36.

Bolton C, Paul C. Glutamate receptors in neuroinflammatory demyelinating disease. Mediators Inflamm 2006; 2006: 93684.

Cammer W, Bloom BR, Norton WT, Gordon S. Degradation of basic protein in myelin by neutral proteases secreted by stimulated macrophages: a possible mechanism of inflammatory demyelination. Proc Natl Acad Sci USA 1978; 75: 1554–8.

Cuzner ML, Gveric D, Strand C, Loughlin AJ, Paemen L, Opdenakker G, et al. The expression of tissue-type plasminogen activator, matrix metalloproteases and endogenous inhibitors in the central nervous system in multiple sclerosis: comparison of stages in lesion evolution. J Neuropathol Exp Neurol 1996; 55: 1194–204.

Cuzner ML, Opdenakker G. Plasminogen activators and matrix metalloproteases, mediators of extracellular proteolysis in inflammatory demyelination of the central nervous system. J Neuroimmunol 1999; 94: 1–14.

Dalmau J, Gleichman AJ, Hughes EG, Rossi JE, Peng X, Lai M, et al. Anti-NMDA-receptor encephalitis: case series and analysis of the effects of antibodies. Lancet Neurol 2008; 7: 1091–8.

Docagne F, Muñetón V, Clemente D, Ali C, Loría F, Correa F, et al. Excitotoxicity in a chronic model of multiple sclerosis: neuroprotective effects of cannabinoids through CB1 and CB2 receptor activation. Mol Cell Neurosci 2007; 34: 551–61.

Fernández-Monreal M, López-Atalaya JP, Benchenane K, Cacquevel M, Dulin F, Le Caer J-P, et al. Arginine 260 of the amino-terminal domain of NR1 subunit is critical for tissue-type plasminogen activator-mediated enhancement of N-methyl-D-aspartate receptor signaling. J Biol Chem 2004; 279: 50850–6.

Floris S, Blezer ELA, Schreibelt G, Döpp E, van der Pol SMA, Schadee-Eestermans IL, et al. Blood-brain barrier permeability and monocyte infiltration in experimental allergic encephalomyelitis: a quantitative MRI study. Brain 2004; 127: 616–27.

Garg SK, Banerjee R, Kipnis J. Neuroprotective immunity: T cell-derived glutamate endows astrocytes with a neuroprotective phenotype. J Immunol 2008; 180: 3866–73.

Gleichman AJ, Spruce LA, Dalmau J, Seeholzer SH, Lynch DR. Anti-NMDA receptor encephalitis antibody binding is dependent on amino acid identity of a small region within the GluN1 amino terminal domain. J Neurosci 2012; 32: 11082–94.

Kamat PK, Kalani A, Tyagi SC, Tyagi N. Hydrogen sulfide epigenetically attenuates homocysteine-induced mitochondrial toxicity mediated through NMDA receptor in mouse brain endothelial (bEnd3) cells. J Cell Physiol 2015; 230: 378–94.

Kooij G, Kroon J, Paul D, Reijerkerk A, Geerts D, van der Pol SMA, et al. P-glycoprotein regulates trafficking of CD8(+) T cells to the brain parenchyma. Acta Neuropathol 2014; 127: 699–711.

Lee M, Suk K, Kang Y, McGeer E, McGeer PL. Neurotoxic factors released by stimulated human monocytes and THP-1 cells. Brain Res 2011; 1400: 99–111.

Lin L, Jin Y, Mars WM, Reeves WB, Hu K. Myeloid-derived tissue-type plasminogen activator promotes macrophage motility through FAK, Rac1, and NF-κB pathways. Am J Pathol 2014; 184: 2757–67.

Lopes Pinheiro MA, Kooij G, Mizee MR, Kamermans A, Enzmann G, Lyck R, et al. Immune cell trafficking across the barriers of the central nervous system in multiple sclerosis and stroke. Biochim Biophys Acta 2016; 1862: 461–71

Macrez R, Obiang P, Gauberti M, Roussel B, Baron A, Parcq J, et al. Antibodies preventing the interaction of tissue-type plasminogen activator with N-methyl-D-aspartate receptors reduce stroke damages and extend the therapeutic window of thrombolysis. Stroke 2011; 42: 2315–22.

Manning SM, Talos DM, Zhou C, Selip DB, Park H-K, Park C-J, et al. NMDA receptor blockade with memantine attenuates white matter injury in a rat model of periventricular leukomalacia. J Neurosci 2008; 28: 6670–8.

Mantuano E, Lam MS, Gonias SL. LRP1 assembles unique co-receptor systems to initiate cell signaling in response to tissue-type plasminogen activator and myelin-associated glycoprotein. J Biol Chem 2013; 288: 34009–18.

Mikasova L, De Rossi P, Bouchet D, Georges F, Rogemond V, Didelot A, et al. Disrupted surface cross-talk between NMDA and Ephrin-B2 receptors in anti-NMDA encephalitis. Brain 2012; 135: 1606–21.

Mizee MR, Nijland PG, van der Pol SMA, Drexhage JAR, van Het Hof B, Mebius R, et al. Astrocyte-derived retinoic acid: a novel regulator of blood-brain barrier function in multiple sclerosis. Acta Neuropathol 2014; 128: 691–703.

Moliné-Velázquez V, Cuervo H, Vila-Del Sol V, Ortega MC, Clemente D, de Castro F. Myeloid-derived suppressor cells limit the inflammation by promoting T lymphocyte apoptosis in the spinal cord of a murine model of multiple sclerosis. Brain Pathol 2011; 21: 678–91.

Nicole O, Docagne F, Ali C, Margaill I, Carmeliet P, MacKenzie ET, et al. The proteolytic activity of tissue-plasminogen activator

enhances NMDA receptor-mediated signaling. Nat Med 2001; 7: 59–64.
Obermeier B, Daneman R, Ransohoff RM. Development, maintenance and disruption of the blood-brain barrier. Nat Med 2013; 19: 1584–96.
Pampliega O, Domercq M, Villoslada P, Sepulcre J, Rodríguez-Antigüedad A, Matute C. Association of an EAAT2 polymorphism with higher glutamate concentration in relapsing multiple sclerosis. J Neuroimmunol 2008; 195: 194–8.
Paul C, Bolton C. Modulation of blood-brain barrier dysfunction and neurological deficits during acute experimental allergic encephalomyelitis by the N-methyl-D-aspartate receptor antagonist memantine. J Pharmacol Exp Ther 2002; 302: 50–7.
Pitt D, Werner P, Raine CS. Glutamate excitotoxicity in a model of multiple sclerosis. Nat Med 2000; 6: 67–70.
Polavarapu R, Gongora MC, Yi H, Ranganthan S, Lawrence DA, Strickland D, et al. Tissue-type plasminogen activator-mediated shedding of astrocytic low-density lipoprotein receptor-related protein increases the permeability of the neurovascular unit. Blood 2007; 109: 3270–8.
Reijerkerk A, Kooij G, van der Pol SMA, Leyen T, van Het Hof B, Couraud PO, et al. Tissue-type plasminogen activator is a regulator of monocyte diapedesis through the brain endothelial barrier. J Immunol 2008; 181: 3567–74.
Reijerkerk A, Kooij G, van der Pol SMA, Leyen T, Lakeman K, van Het Hof B, et al. The NR1 subunit of NMDA receptor regulates monocyte transmigration through the brain endothelial cell barrier. J Neurochem 2010; 113: 447–53.
Samson AL, Medcalf RL. Tissue-type plasminogen activator: a multifaceted modulator of neurotransmission and synaptic plasticity. Neuron 2006; 50: 673–8.
Scott GS, Bowman SR, Smith T, Flower RJ, Bolton C. Glutamate-stimulated peroxynitrite production in a brain-derived endothelial cell line is dependent on N-methyl-D-aspartate (NMDA) receptor activation. Biochem Pharmacol 2007; 73: 228–36.
Sharp CD, Hines I, Houghton J, Warren A, Jackson TH, Jawahar A, et al. Glutamate causes a loss in human cerebral endothelial barrier integrity through activation of NMDA receptor. Am J Physiol Heart Circ Physiol 2003; 285: H2592–8.
Skerry TM, Genever PG. Glutamate signalling in non-neuronal tissues. Trends Pharmacol Sci 2001; 22: 174–81.
Sulkowski G, Dąbrowska-Bouta B, Chalimoniuk M, Strużyńska L. Effects of antagonists of glutamate receptors on pro-inflammatory cytokines in the brain cortex of rats subjected to experimental autoimmune encephalomyelitis. J Neuroimmunol 2013; 261: 67–76.
Suzuki Y, Nagai N, Yamakawa K, Kawakami J, Lijnen HR, Umemura K. Tissue-type plasminogen activator (t-PA) induces stromelysin-1 (MMP-3) in endothelial cells through activation of lipoprotein receptor-related protein. Blood 2009; 114: 3352–8.
Tremolizzo L, DiFrancesco JC, Rodriguez-Menendez V, Sirtori E, Longoni M, Cassetti A, et al. Human platelets express the synaptic markers VGLUT1 and 2 and release glutamate following aggregation. Neurosci Lett 2006; 404: 262–5.
Uhl B, Zuchtriegel G, Puhr-Westerheide D, Praetner M, Rehberg M, Fabritius M, et al. Tissue plasminogen activator promotes postischemic neutrophil recruitment via its proteolytic and nonproteolytic properties. Arterioscler Thromb Vasc Biol 2014; 34: 1495–504.
Verkhratsky A, Kirchhoff F. NMDA Receptors in glia. Neuroscientist 2007; 13: 28–37.
Wang J, Zhang X, Mu L, Zhang M, Gao Z, Zhang J, et al. t-PA acts as a cytokine to regulate lymphocyte-endothelium adhesion in experimental autoimmune encephalomyelitis. Clin Immunol 2014; 152: 90–100.
Wang S, Lee S-R, Guo S-Z, Kim WJ, Montaner J, Wang X, et al. Reduction of tissue plasminogen activator-induced matrix metalloproteinase-9 by simvastatin in astrocytes. Stroke 2006; 37: 1910–12.
Wang X, Lee S-R, Arai K, Lee S-R, Tsuji K, Rebeck GW, et al. Lipoprotein receptor-mediated induction of matrix metalloproteinase by tissue plasminogen activator. Nat Med 2003; 9: 1313–17.
Weksler BB, Subileau EA, Perrière N, Charneau P, Holloway K, Leveque M, et al. Blood-brain barrier-specific properties of a human adult brain endothelial cell line. FASEB J 2005; 19: 1872–74.